Limit Cycle Oscillation of a Fluttering Cantilever Plate

Ye Weiliang*
Nanjing Aeronautical Institute, Nanjing, People's Republic of China
and
Earl Dowell†
Duke University, Durham, North Carolina 27706

This is the first such study for a plate with some edges unsupported. Previous work has dealt with all edges supported. Von Karman theory for a plate and quasisteady, supersonic aerodynamic theory have been assumed. A Rayleigh-Ritz approach has been used to solve for the nonlinear oscillation of a fluttering plate. The length-to-width ratio of the cantilever plate has a significant effect on the flutter vibration. For small length-to-width ratio, the dominant chordwise modes are translation and rotation; however, higher bending modes must be included to obtain an accurate prediction of the flutter onset and limit cycle oscillation. For large length-to-width ratio, significant chordwise bending is apparent in the flutter motion, with the trailing edge area having the largest motion.

Nomenclature

a, b	= generalized coordinates
c	= chord of plate
D	= plate stiffness
E	= modulus of elasticity
h	= plate thickness
$L,\ L = T - U$	= plate width, Lagrangian
M	= Mach number
$m,\ m = \rho_m h$	= mode number, panel mass/area
n	= mode number
Δp	= (aerodynamic) pressure loading on panel
Q	= generalized (aerodynamic) force
q	= generalized coordinate
$q = \rho_\infty V_\infty^2/2$	= dynamic pressure
T	= kinetic energy
t	= time
U	= elastic energy
u, v	= in-plane displacements
V_∞	= fluid velocity
w	= plate transverse deflection
x	= streamwise coordinate
y	= spanwise coordinate
z	= normal coordinate
$\beta = \sqrt{M^2 - 1}$	= compressibility correction factor
$\lambda = \dfrac{\rho_\infty V_\infty^2 c^3}{D}$	= nondimensional dynamic pressure
$\mu = \dfrac{\rho_\infty c}{\rho_m h}$	= nondimensional mass ratio
ν	= Poisson's ratio
ρ_∞, ρ_m	= air density, plate density
$\tau = t\sqrt{\dfrac{D}{m c^4}}$	= nondimensional time
ϕ	= mode function
ψ	= mode function
ω	= frequency
$(\dot{}), (\,)'$	= $\dfrac{\mathrm{d}(\,)}{\mathrm{d}\tau}$ or $\dfrac{\mathrm{d}(\,)}{\mathrm{d}t}$, $\dfrac{\mathrm{d}(\,)}{\mathrm{d}(x/c)}$ or $\dfrac{\mathrm{d}(\,)}{\mathrm{d}(y/L)}$

Received Sept. 5, 1990; revision received May 15, 1991; accepted for publication June 4, 1991.

*Visiting Fellow; Associate Professor on leave from Nanjing Aeronautical Institute, Department of Aerodynamics.
†Dean, School of Engineering. Fellow AIAA.

Introduction

CONSIDERED here is the response of a cantilever plate in high supersonic flow to a disturbance (Fig. 1). In earlier work, Dowell and others have studied the nonlinear oscillation of a simply supported or clamped fluttering plate by the use of Galerkin's method.[1,2] In the present work, the nonlinear oscillations of a cantilever plate have been investigated by the use of a Rayleigh-Ritz approach. The Rayleigh-Ritz approach represents the plate deflection as a series of mode functions of several variables. The mode functions only satisfy the geometric boundary conditions. This approach can be used to reduce the description of the plate motion to a system of nonlinear ordinary differential equations in time which are solved by numerical integration. The Runge-Kutta method has been used to solve the nonlinear equations in time.

Within the framework of linear plate theory, there is a value of flow dynamic pressure above which the plate motion is unstable, and the response grows exponentially with time. However, the nonlinear membrane forces induced by the plate motion limit the plate amplitude. These nonlinear forces will be included in the elastic strain energy equations. The nonlinear term is from the stretching energy. Quasisteady (linear) aerodynamic theory is employed as appropriate to high speeds, i.e., piston theory.

In the present work, there are several notable features to the analysis:

1) No particular support conditions have been specified. Any support condition can be handled. In this paper, a cantilever plate has been studied.

2) No essential limitation is placed on the number of modes employed. Up to 10 modes along the airflow direction and three modes along the span direction have been used. Convergence of the Rayleigh-Ritz method has been assured.

3) All limit cycle oscillations in time are obtained by a numerical Runge-Kutta method. The amplitude, shape, and frequency of the oscillations can be examined in detail. Harmonic limit cycle oscillation may be studied, as well as aperiodic motion.

4) The effects of dynamic pressure and other parameters on the limit cycle deflection and frequency can be evaluated from the numerical results.

Theoretical Analysis

The Rayleigh-Ritz method consists of assuming the form of the unknown solution in terms of known functions (trial functions) with unknown adjustable parameters. Here, the mode functions satisfy the geometric boundary conditions.

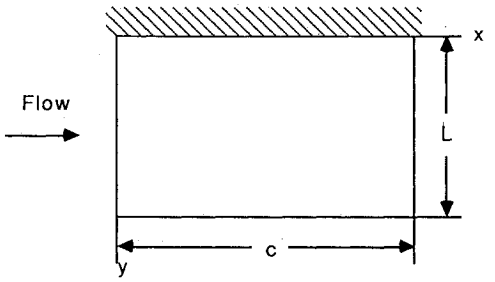

Fig. 1 Plate geometry.

Energy Expressions

For a plate, the elastic energy U is given by

$$U = U_S + U_B \tag{1}$$

where U_S is the stretching energy and U_B is the bending energy. U_S and U_B may be expressed in terms of the displacements u, v, and w:

$$U_S = \frac{E\,h}{2(1-\nu^2)} \iint \left\{ \left[\frac{\partial u}{\partial x} + \frac{1}{2}\left(\frac{\partial w}{\partial x}\right)^2 \right]^2 + \left[\frac{\partial v}{\partial y} + \frac{1}{2}\left(\frac{\partial w}{\partial y}\right)^2 \right]^2 + 2\nu \left[\frac{\partial u}{\partial x} + \frac{1}{2}\left(\frac{\partial w}{\partial x}\right)^2 \right] * \left[\frac{\partial v}{\partial y} + \frac{1}{2}\left(\frac{\partial w}{\partial y}\right)^2 \right] + \frac{(1-\nu)}{2} \left[\frac{\partial v}{\partial x} + \frac{\partial u}{\partial y} + \frac{\partial w}{\partial x}\frac{\partial w}{\partial y} \right]^2 \right\} dx\,dy \tag{2}$$

$$U_B = \frac{D}{2} \iint \left[\left(\frac{\partial^2 w}{\partial x^2}\right)^2 + \left(\frac{\partial^2 w}{\partial y^2}\right)^2 + 2\nu \frac{\partial^2 w}{\partial x^2}\frac{\partial^2 w}{\partial y^2} + 2(1-\nu)\left(\frac{\partial^2 w}{\partial x \partial y}\right)^2 \right] dx\,dy \tag{3}$$

The kinetic energy is

$$T = \frac{1}{2} \iint m \left(\frac{\partial w}{\partial t}\right)^2 dx\,dy \tag{4}$$

Mode Functions

Expand the three displacements as

$$u = \sum_i \sum_j a_{ij}(t) u_i(x) v_j(y) \tag{5}$$

$$v = \sum_r \sum_s b_{rs}(t) u_r(x) v_s(y) \tag{6}$$

$$w = \sum_m \sum_n q_{mn}(t) \phi_m(x) \psi_n(y) \tag{7}$$

where the mode functions are

$$u_i(x) = \cos i\pi \frac{x}{c} \qquad v_j(y) = \sin\left(\frac{2j-1}{2}\right)\pi \frac{y}{L} \tag{8}$$

$$u_r(x) = \cos r\pi \frac{x}{c} \qquad v_s(y) = \sin\left(\frac{2s-1}{2}\right)\pi \frac{y}{L} \tag{9}$$

$$\phi_m(x) = \sqrt{2}\sin\left(\beta_m \frac{x}{c} + \frac{3}{4}\pi\right) + \exp\left(-\beta_m \frac{x}{c}\right) + (-1)^{m+1} \exp\left[-\beta_m\left(1 - \frac{x}{c}\right)\right] \tag{10}$$

$$\psi_n(y) = \sqrt{2}\sin\left(\beta_n \frac{y}{L} - \frac{1}{4}\pi\right) + \exp\left(-\beta_n \frac{y}{L}\right) + (-1)^{n+1} \exp\left[-\beta_n\left(1 - \frac{y}{L}\right)\right] \tag{11}$$

with

$$\beta_m = (m - \tfrac{3}{2})\pi \text{ and } \beta_n = (n - \tfrac{1}{2})\pi$$

$\phi_m(x)$ is a free-free beam function and $\psi_n(y)$ is a cantilever beam function taken from Ref. 3 (also see Ref. 4). For $m < 2$, the translation and the rigid rotation modes are employed. Thus

$$\phi_1(x) = A \text{ and } \phi_2(x) = A\left(1 - 2\frac{x}{c}\right)$$

where $A = 2$ is chosen in order that the value of $\phi_1(x)$ and $\phi_2(x)$ at $x = 0$ be consistent with the value of function $\phi_m(x)$ at $x = 0$ for $m > 2$. All mode functions satisfy the geometric boundary conditions; at $y = 0$, $v_j(y) = 0$, $v_s(y) = 0$ and $\psi_n(y) = d\psi_n(y)/dy = 0$. Therefore, $u = 0$, $v = 0$, and $w = \partial w/\partial y = 0$.

Lagrange's Equations

These are

$$\frac{\partial L}{\partial a_{ij}} = 0 \tag{12a}$$

$$\frac{\partial L}{\partial b_{rs}} = 0 \tag{12b}$$

$$\frac{d}{dt}\left(\frac{\partial L}{\partial \dot{q}_{mn}}\right) - \frac{\partial L}{\partial q_{mn}} + Q_{mn} = 0 \tag{12c}$$

where $L = T - U$ and Q_{mn} is generalized force, i.e.

$$Q_{mn} = \iint \Delta p(x,y,t) \frac{\partial w}{\partial q_{mn}} dx\,dy \tag{13}$$

The aerodynamic pressure loading Δp will be assumed to be that of quasisteady, supersonic theory[1]

$$\Delta p = \frac{2q}{\beta}\left[\frac{\partial w}{\partial x} + \frac{M^2 - 2}{M^2 - 1}\frac{1}{V_\infty}\frac{\partial w}{\partial t}\right] \tag{14}$$

Note that in Eq. (14), the flow has been taken to be over one side of the plate only. For flow over both sides of the plate, Δp is twice the value given by Eq. (14).

Substituting $L = T - U$ into Eq. (12), we have

$$\frac{\partial U_S}{\partial a_{ij}} = 0 \tag{15a}$$

$$\frac{\partial U_S}{\partial b_{rs}} = 0 \tag{15b}$$

$$\frac{d}{dt}\left(\frac{\partial T}{\partial \dot{q}_{mn}}\right) + \frac{\partial U_B}{\partial q_{mn}} + \frac{\partial U_S}{\partial q_{mn}} + Q_{mn} = 0 \tag{15c}$$

Nondimensional Equations of Motion

Substitute Eqs. (5), (6), and (7) into Eq. (2), substitute Eq. (2) into Eq. (15a) and then employ appropriate nondimensionalization, i.e., $\bar{a}_{ij} = a_{ij}/h$, $\bar{b}_{rs} = b_{rs}/h$, $\bar{q}_{mn} = q_{mn}/h$, $\bar{u} =$

u/h, $\bar{v} = v/h$, $\bar{w} = w/h$, $\bar{x} = x/c$, and $\bar{y} = y/L$. The overbar is then dropped for convenience. Thus,

$$\sum_k \sum_p C_{kp}^{ij} a_{kp} + \sum_g \sum_f C_{gf}^{ij} b_{gf} = C^{ij} \tag{16}$$

or in matrix form

$$[C_a]\{a\} + [C_b]\{b\} = \{C\} \tag{17}$$

where

$$C_{kp}^{ij} = 2\left(\frac{h}{c}\right)^2 \int_0^1 u_k' u_i' \, dx \int_0^1 v_p v_j \, dy + (1 - \nu)\left(\frac{h}{L}\right)^2 \int_0^1 u_k u_i \, dx \int_0^1 v_p' v_j' \, dy \tag{18}$$

$$C_{gf}^{ij} = 2\nu \frac{h^2}{cL} \int_0^1 u_g u_i' \, dx \int_0^1 v_f' v_j \, dy + (1 - \nu) \frac{h^2}{cL} \int_0^1 u_g' u_i \, dx \int_0^1 v_f v_j' \, dy \tag{19}$$

$$C^{ij} = -\sum_m \sum_n \sum_p \sum_l q_{mn} q_{pl} \left(\frac{h}{c}\right)^3 \times \int_0^1 \phi_m' \phi_p' u_i' \, dx \int_0^1 \psi_n \psi_l v_j \, dy - \nu\left(\frac{h}{L}\right)^2 \left(\frac{h}{c}\right) \sum_m \sum_n \sum_p \sum_l q_{mn} q_{pl} \times \int_0^1 \phi_m \phi_p u_i' \, dx \int_0^1 \psi_n' \psi_l' v_j \, dy - (1 - \nu)\left(\frac{h}{L}\right)^2 \left(\frac{h}{c}\right) \sum_m \sum_n \sum_p \sum_l q_{mn} q_{pl} \times \int_0^1 \phi_m' \phi_p u_i \, dx \int_0^1 \psi_n \psi_l' v_j' \, dy \tag{20}$$

Substituting Eq. (2) into Eq. (15b), we have

$$\sum_k \sum_p D_{kp}^{rs} a_{kp} + \sum_g \sum_f D_{gf}^{rs} b_{gf} = D^{rs} \tag{21}$$

That is

$$[D_a]\{a\} + [D_b]\{b\} = \{D\} \tag{22}$$

where

$$D_{kp}^{rs} = 2\nu \frac{h^2}{cL} \int_0^1 u_k' u_r \, dx \int_0^1 v_p v_s' \, dy + (1 - \nu) \frac{h^2}{cL} \int_0^1 u_k u_r' \, dx \int_0^1 v_p' v_s \, dy \tag{23}$$

$$D_{gf}^{rs} = 2\left(\frac{h}{L}\right)^2 \int_0^1 u_g u_r \, dx \int_0^1 v_f' v_s' \, dy + (1 - \nu) \left(\frac{h}{c}\right)^2 \int_0^1 u_g' u_r' \, dx \int_0^1 v_f v_s \, dy \tag{24}$$

$$D^{rs} = -\sum_m \sum_n \sum_p \sum_l q_{mn} q_{pl} \left(\frac{h}{L}\right)^3 \times \int_0^1 \phi_m \phi_p u_r \, dx \int_0^1 \psi_n' \psi_l' v_s' \, dy - \nu\left(\frac{h}{L}\right)\left(\frac{h}{c}\right)^2 \sum_m \sum_n \sum_p \sum_l q_{mn} q_{pl} \times \int_0^1 \phi_m' \phi_p' u_r \, dx \int_0^1 \psi_n \psi_l v_s' \, dy - (1 - \nu)\left(\frac{h}{L}\right)\left(\frac{h}{c}\right)^2 \sum_m \sum_n \sum_p \sum_l q_{mn} q_{pl} \times \int_0^1 \phi_m' \phi_p u_r' \, dx \int_0^1 \psi_n \psi_l' v_s \, dy \tag{25}$$

Equations (17) and (22) are algebraic relations that may be solved (simultaneously) for a_{ij} and b_{rs} in terms of q_{mn}. That is

$$\begin{bmatrix} C_a & C_b \\ D_a & D_b \end{bmatrix} \begin{Bmatrix} a \\ b \end{Bmatrix} = \begin{Bmatrix} C \\ D \end{Bmatrix} \tag{26}$$

Substituting Eqs. (2), (3), and (4) into Eq. (15c) and employing appropriate nondimensionalization, we have

$$\sum_m \sum_n [A_{mn}^{ij} \ddot{q}_{mn}(\tau) + B_{mn}^{ij} q_{mn}(\tau)] + F^{ij} + Q^{ij} = 0 \tag{27}$$

That is

$$[A]\{\ddot{q}\} + [B]\{q\} + \{F\} + \{Q\} = 0 \tag{28}$$

where

$$A_{mn}^{ij} = \frac{1}{6} \int_0^1 \phi_m \phi_i \, dx \int_0^1 \psi_n \psi_j \, dy \tag{29}$$

$$B_{mn}^{ij} = \frac{1}{6} \left\{ \int_0^1 \phi_m'' \phi_i'' \, dx \int_0^1 \psi_n \psi_j \, dy + \left(\frac{c}{L}\right)^4 \int_0^1 \phi_m \phi_i \, dx \int_0^1 \psi_n'' \psi_j'' \, dy + \nu\left(\frac{c}{L}\right)^2 \left[\int_0^1 \phi_m \phi_i'' \, dx \int_0^1 \psi_n'' \psi_j \, dy + \int_0^1 \phi_m'' \phi_i \, dx \int_0^1 \psi_n \psi_j'' \, dy \right] + 2(1 - \nu)\left(\frac{c}{L}\right)^2 \int_0^1 \phi_m' \phi_i' \, dx \int_0^1 \psi_n' \psi_j' \, dy \right\} \tag{30}$$

$$Q^{ij} = \frac{\lambda}{6\beta} \left[\sum_m \sum_n q_{mn}(\tau) \int_0^1 \phi_m' \phi_i \, dx \int_0^1 \psi_n \psi_j \, dy + \frac{M^2 - 2}{M^2 - 1} \sqrt{\frac{\mu}{\lambda}} \sum_m \sum_n \dot{q}_{mn}(\tau) \int_0^1 \phi_m \phi_i \, dx \int_0^1 \psi_n \psi_j \, dy \right] \tag{31}$$

Note again that for flow over both sides of the plate ρ_∞ should be replaced by $2\rho_\infty$ in the definitions of λ and μ.

F^{ij} is given in the Appendix.

Multiply Eq. (28) by the inverse of matrix A. Thus,

$$\{\ddot{q}\} + [A]^{-1}[B]\{q\} + [A]^{-1}\{F\} + [A]^{-1}\{Q\} = 0 \tag{32}$$

Note that the F^{ij} term is a nonlinear term and the Q^{ij} involves q_{mn} and $\dot{q}_{mn}$. Equation (27) is a nonlinear ordinary differential equation. It can be solved numerically by the Runge-Kutta method.

Numerical Procedures and Results

Equation (32) is a set of nonlinear ordinary differential equations. Note that the nonlinear terms F^{ij} include not only the generalized coordinates, q_{mn}, but also a_{ij} and b_{rs}. Equations (17) and (22) are algebraic equations. If q_{mn} is given, the generalized coordinates a_{ij} and b_{rs} obtained from Eqs. (17)

and (22) can be substituted into Eq. (32). Then Eq. (32) can be solved by the Runge-Kutta method, step by step in time. The panel response to the initial condition can thus be obtained. The time step has to be adjusted to the number of modes retained in the calculation because of the sensitivity of the stability of the time marching method to the time step. For example, with eight modes along the chord direction or six modes along the chord direction and two modes along the span direction, the time step has to be less than 0.005. In all results reported here, $M = 2$, $\mu = 0.1$, and $\nu = 0.33$.

Limit Cycle Response of Cantilever Plate

Plots of panel deflection (at $x = 0.75c$ and $y = L$) vs time for two dynamic pressures are presented in Fig. 2. The amplitude of the nonlinear vibration tends toward a constant as time increases. A limit cycle oscillation for the case of six modes along the chord direction and two modes along the span direction is reached after $\tau > 1$. In a linear model, for a given initial disturbance, the panel motion may decrease with time or it may increase. In Fig. 3 are shown plots of panel deflection vs time (at $x = 0.75c$) without the nonlinear stretching force. The vibration increases rapidly when the dynamic pressure is greater than the dynamic pressure for flutter onset (see Figs. 3a and 3b). For dynamic pressure less than the onset value, the deflection response decays with time in either the linear (see Fig. 3c) or nonlinear model.

Convergence of Modal Expansion

Figure 4 displays the peak amplitude of the limit cycle for various dynamic pressures for a square plate, $c/L = 1$. The amplitude of the limit cycle increases as the dynamic pressure increases. Also shown in Fig. 4 is the effect of the number of modes retained in the calculation on the amplitude of the limit cycle. The amplitude for six modes along the flow direction combined with one mode along the span direction is close to that for eight modes, but quite different from that for four modes along the flow direction. In Fig. 5, the number of modes along the span direction has been varied. The results of two modes along the span direction combined with four modes along the flow direction is near that of three modes along the span direction, but quite different from that of one mode along the span direction. In Fig. 6 are shown the results of six modes along the flow direction combined with two modes along the span direction, which are compared with those of six modes (x) and one mode (y). In Fig. 7 is shown a comparison of the results of six modes (x) and two modes (y) with those of four modes (x) and two modes (y). Obviously, the results of four modes (x) and two modes (y) are near those of six modes (x) and two modes (y). Generally, it

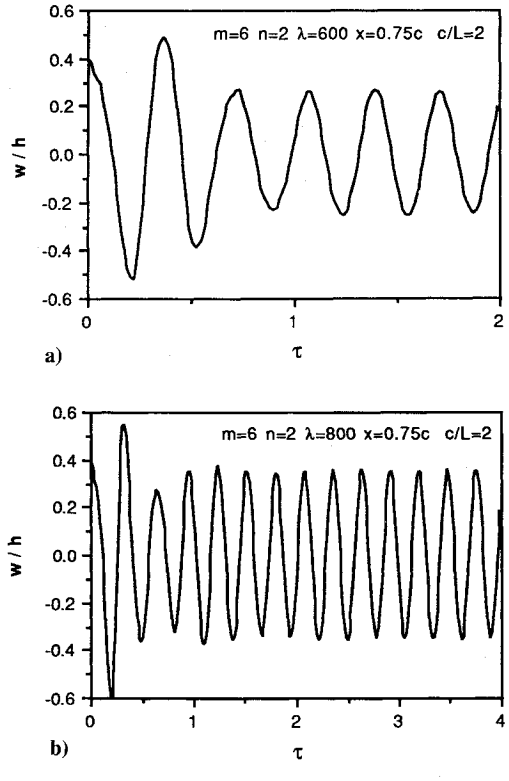

Fig. 2 Deflection vs time.

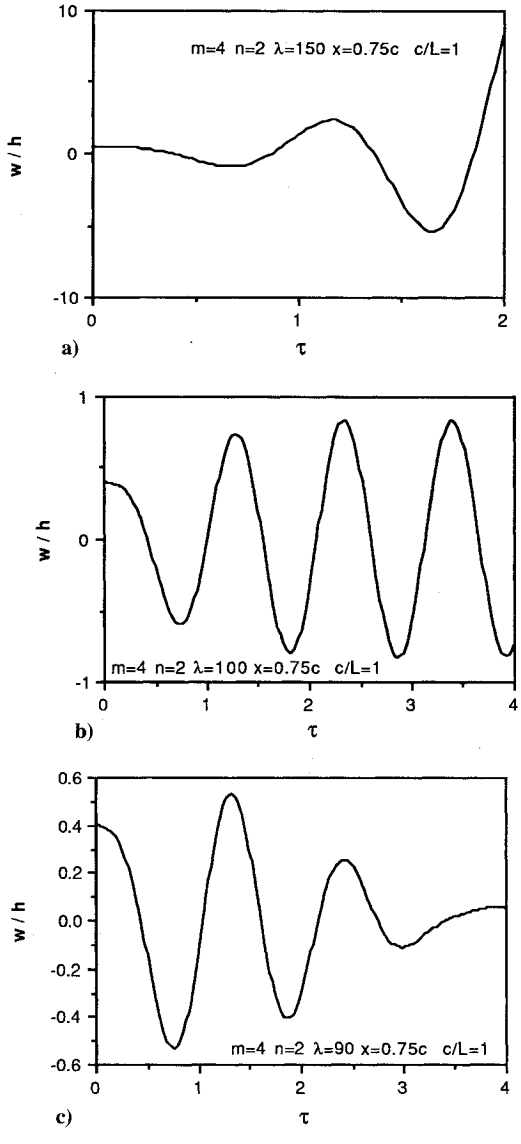

Fig. 3 Deflection vs time.

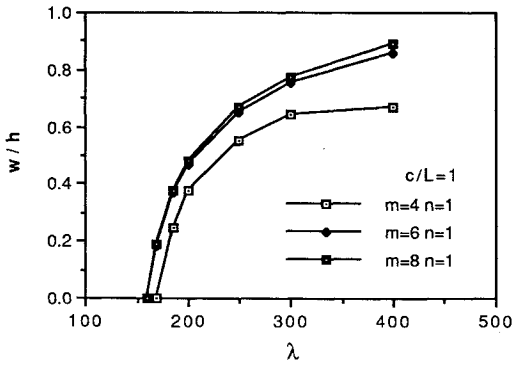

Fig. 4 Peak deflection vs dynamic pressure.

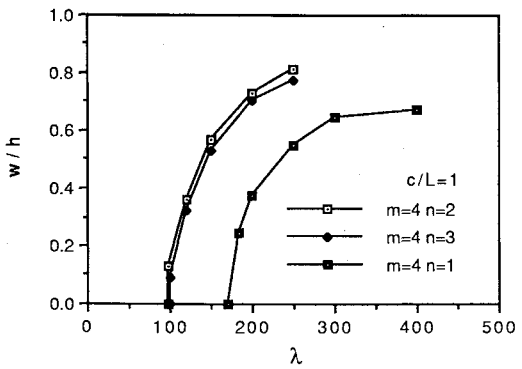

Fig. 5 Peak deflection vs dynamic pressure.

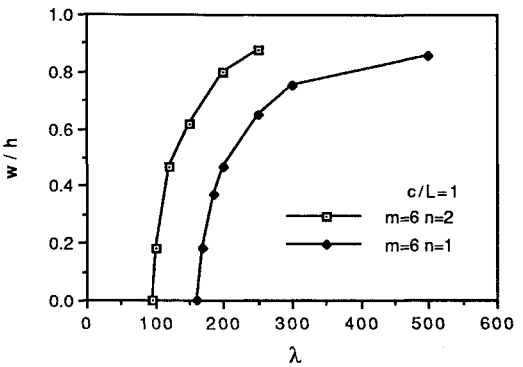

Fig. 6 Peak deflection vs dynamic pressure.

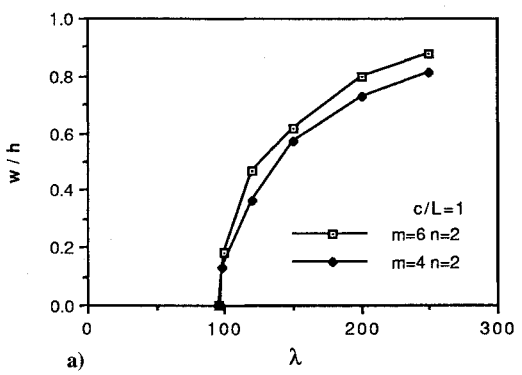

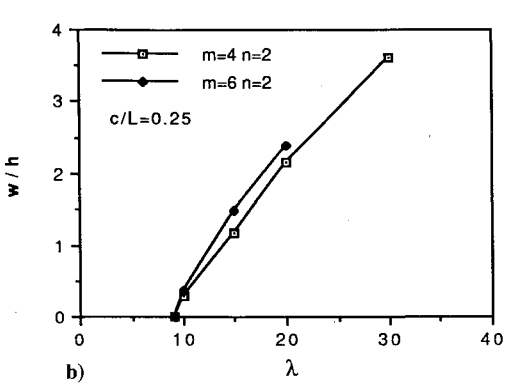

Fig. 7 Peak deflection vs dynamic pressure.

is concluded that six modes along the flow direction and two modes along the span direction can be used for an accurate calculation for a length-to-width ratio of less than 4. This conclusion is based upon extensive calculations of results for various c/L, similar to those of Figs. 4–7 for $c/L = 1$.

It is worthy of note that retaining only two modes in the flow direction gives no flutter at any λ for any c/L. This is a well-known result from classical wing flutter theory.[5]

Effect of Length-to-Width Ratio

In Fig. 8a is given limit cycle amplitude vs dynamic pressure for a length-to-width ratio of 2 with different numbers of modes along the flow direction. It is seen that the amplitude for six modes along the flow direction is close to that for eight modes, but quite different from that for four modes. Also in Fig. 8b it is shown that the amplitude for six modes is near the amplitude for eight modes for a panel length-to-width ratio of 4, and the amplitude for eight modes is even closer to that for 10 modes. In Fig. 8c is shown the amplitude for 8 and 10 modes for a length-to-width ratio of 10. Generally, a

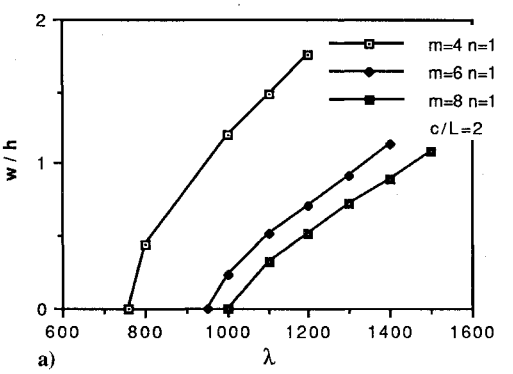

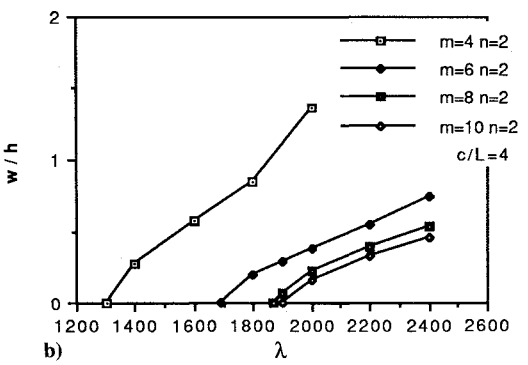

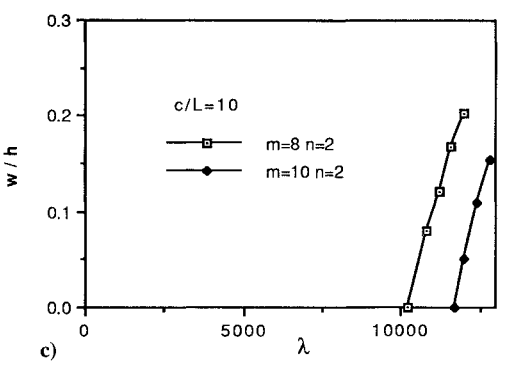

Fig. 8 Study of modal convergence: peak deflection vs dynamic pressure.

large number of modes along the flow direction is needed as the panel length-to-width ratio increases.

In Fig. 9 is shown the amplitude vs dynamic pressure for plate length-to-width ratios 0.25, 0.5, 1, and 2 with six modes (x) and two modes (y). The growth rate of the amplitude as the dynamic pressure increases for a panel length-to-width ratio of 2 is substantially less than that for a panel length-to-width ratio of 1, 0.5, and 0.25. This, as will be seen below, is a result of the greater chordwise bending and hence plate-like behavior for larger c/L.

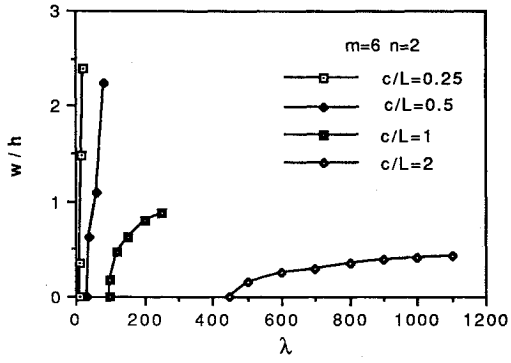

Fig. 9 Peak deflection vs dynamic pressure.

Deflection Shape

In Fig. 10, the chordwise shape of the limit cycle panel deflection for various dynamic pressures, λ, and length-to-width ratios, c/L, are given. From the plots, the shape of the deflection is seen to be dominated by the translation and rotation modes for small to moderate c/L. The translation motion is the main component of the motion when the dynamic pressure and the length-to-width ratio are small. For example, see $\lambda = 50$ and $c/L = 0.5$ in Fig. 10a and $\lambda = 250$ and $c/L = 1$ in Fig. 10b. The component of the rotation motion increases gradually as the dynamic pressure and the length-to-width ratio increase, e.g., $\lambda = 900$ and $c/L = 2$ in Fig. 10(c). Also for larger λ and c/L, although the rigid body modes remain dominant up to $c/L = 2$, the bending modes become more important. For example, see Fig. 10d where $\lambda = 2400$ and $c/L = 4$ and Fig. 10e where $\lambda = 12000$ and $c/L = 10$. Note that in the latter the dominant deflection is near the trailing edge.

Recall again, however, that retaining only the translation and rotation modes in the analysis precludes flutter. Thus the bending modes are essential to describing the flutter phenomenon for all c/L.

Generalized Coordinate Contribution

The magnitudes of the generalized coordinates for different modes are presented in Fig. 11. From the plots, the gener-

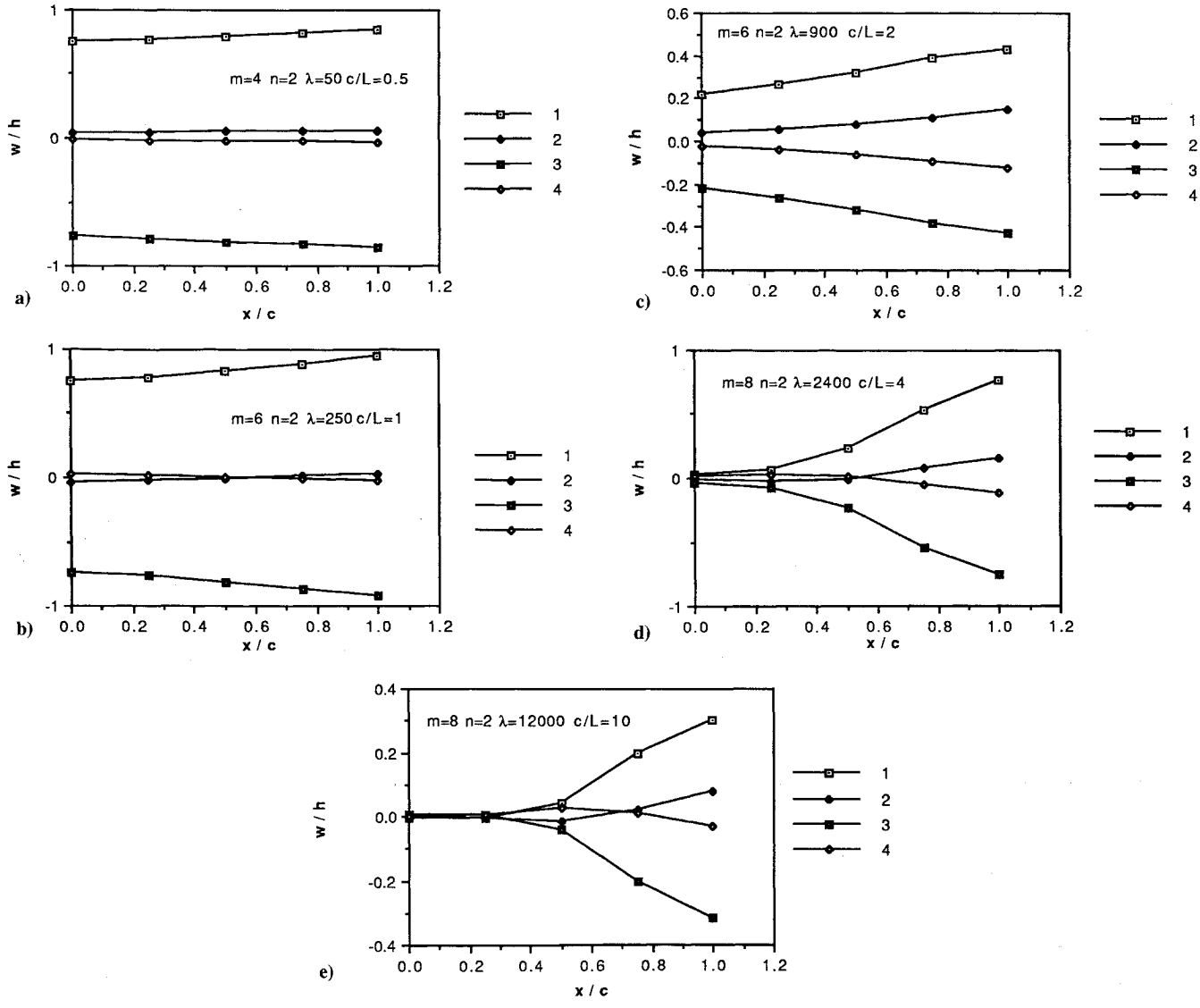

Fig. 10 Deflection vs streamwise position for four times during a limit cycle of oscillation.

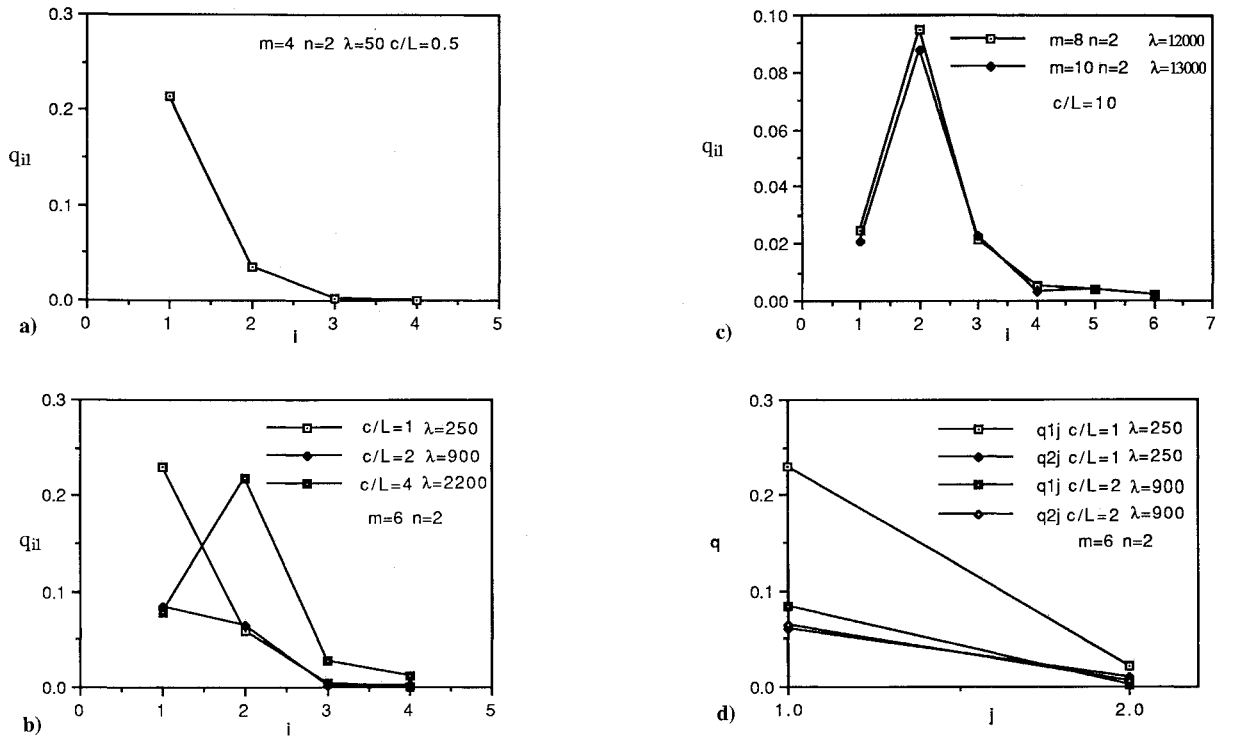

Fig. 11 Generalized coordinate vs mode number in flow direction (a–c) and in spanwise direction (d).

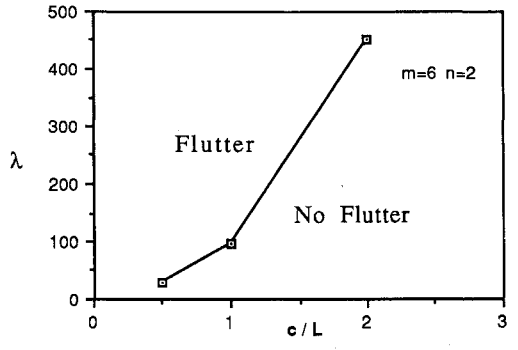

Fig. 12 Flutter boundary: dynamic pressure vs length-to-width ratio.

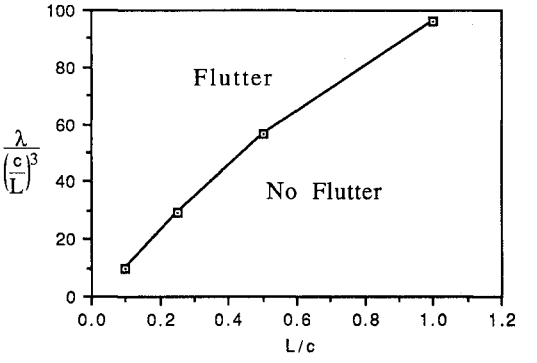

Fig. 13 Flutter boundary: dynamic pressure vs width-to-length ratio.

alized coordinates of the translation and rotation modes are greater than those of other modes for small to moderate length-to-width ratios. The generalized coordinate of the first mode is the main component of nonlinear vibration for the case of $\lambda = 50$ and $c/L = 0.5$ in Fig. 11a. Figure 11b shows the effect of length-to-width ratio on the generalized coordinate contribution. The generalized coordinate of the second mode becomes important as the panel length-to-width ratio increases. Figure 11c shows the generalized coordinate for different mode combinations along the flow direction for a length-to-width ratio of 10. In Fig. 11d are shown the generalized coordinates of the first and second modes along the span direction when $c/L = 1$ and 2. The generalized coordinate of the second mode along the span direction is substantially less than that of the first mode, but the contribution of the second mode to the amplitude cannot always be neglected. In Fig. 6 recall the effect of the second mode along the span direction on the amplitude of the limit cycle oscillation. Compared with the case of only the first mode along the span direction, the flutter results are changed measurably.

Determination of Flutter Onset

The flutter onset for a cantilever plate may be determined from the intersection of the limit cycle amplitude curves with the dynamic pressure axis. For example, Fig. 4 shows the dynamic pressure of flutter onset for $c/L = 1$ and various numbers of modes retained in the calculation. The flutter dynamic pressure λ for four modes (x) and one mode (y) is about 170. This value was independently confirmed by the results from a *linear* flutter analysis (not shown).

In Fig. 12, the λ for the onset of flutter, λ_F, is plotted vs c/L ratios. These results were obtained from nonlinear theory with aerodynamic damping included. On physical grounds and from the results of Fig. 12, it appears that $\lambda_F \to 0$ as $c/L \to 0$.

The flutter boundary, in another form, is shown also in Fig. 13. Here the abscissa is L/c and the ordinate is $\lambda/(c/L)^3$. Note that the latter is independent of plate chord, c, and only depends upon L (recall the definition of λ). Thus from Fig. 13, the limit as $c/L \to \infty$, or $L/c \to 0$, can be investigated. Again from physical reasoning and Fig. 13, one concludes that $\lambda/(c/L)^3 \to 0$ as $L/c \to 0$.

Conclusions

Although up to 10 modes in the flow direction have been employed in the computation, the generalized coordinate of modes greater than six is very small, in the range of parameters studied. The displacement functions assumed here are suitable for describing the nonlinear flutter vibration of a cantilever plate.

Retaining only two modes in the flow direction precludes the prediction of flutter, even though the lowest modes are most important for nonlinear vibration of a cantilever plate when $c/L < 2$. The shape of the plate deflection appears primarily as a combination of the translation and rotation modes for small to moderate c/L.

The length-to-width ratio for a cantilever plate has a great effect on flutter amplitude of the limit cycle. In particular, as c/L increases, the number of chordwise modes needed to predict flutter increases. For large c/L, substantial chordwise bending occurs in the flutter motion with the dominant deflection occurring near the trailing edge.

This last result means that the effective chord of the plate is substantially less than the physical chord. Hence the effective aerodynamic aspect ratio remains large for $M >> 1$, i.e., $(M^2 - 1)^{1/2}$ times the span divided by the effective chord is substantially greater than unity. Thus two-dimensional, quasi-steady aerodynamic theory remains appropriate for $M >> 1$, even when c/L is large.

Future Work

Several extensions of the work described here are worthy of brief mention. First of all, a more accurate aerodynamic model might be employed. The full linear aerodynamic model could be used, but an interesting and effective next step might be the use of slender wing theory after Fralich and Hedgepeth who used a linear structural model.[6] Another extension would be consideration of thermal stresses, including those sufficient to buckle the platelike wing[7] following Bisplinghoff and Dugundji. Finally, nonrectangular planforms might be considered, e.g., triangular or delta wings.

Appendix: Expression for F^{ij}

The nonlinear term F^{ij} in Eq. (32) is from $\partial U_S/\partial \overline{q}_{ij}$ in Eq. (15c). Thus

$$\frac{\partial U_S}{\partial \overline{q}_{ij}} = \frac{EhcL}{2(1-\nu^2)} \int\int \left\{ 2\left[\frac{h}{c}\frac{\partial \overline{u}}{\partial \overline{x}} + \frac{1}{2}\left(\frac{h}{c}\frac{\partial \overline{w}}{\partial \overline{x}}\right)^2 \right]\left(\frac{h}{c}\right)^2 \left(\frac{\partial \overline{w}}{\partial \overline{x}}\right)\phi_i'\psi_j \right.$$
$$+ 2\left[\frac{h}{L}\frac{\partial \overline{v}}{\partial \overline{y}} + \frac{1}{2}\left(\frac{h}{L}\frac{\partial \overline{w}}{\partial \overline{y}}\right)^2 \right]\left(\frac{h}{L}\right)^2 \left(\frac{\partial \overline{w}}{\partial \overline{y}}\right)\phi_i\psi_j' + 2\nu\left[\frac{h}{c}\frac{\partial \overline{u}}{\partial \overline{x}} \right.$$
$$+ \frac{1}{2}\left(\frac{h}{c}\frac{\partial \overline{w}}{\partial \overline{x}}\right)^2 \left]\left(\frac{h}{L}\right)^2 \left(\frac{\partial \overline{w}}{\partial \overline{y}}\right)\phi_i\psi_j' + 2\nu\left[\frac{h}{L}\frac{\partial \overline{v}}{\partial \overline{y}} \right.\right.$$
$$+ \frac{1}{2}\left(\frac{h}{L}\frac{\partial \overline{w}}{\partial \overline{y}}\right)^2 \left]\left(\frac{h}{c}\right)^2 \left(\frac{\partial \overline{w}}{\partial \overline{x}}\right)\phi_i'\psi_j + (1-\nu)\frac{h^2}{cL}\left[\frac{h}{c}\frac{\partial \overline{v}}{\partial \overline{x}} \right.\right.$$
$$\left.\left. + \frac{h}{L}\frac{\partial \overline{u}}{\partial \overline{y}} + \frac{h^2}{cL}\frac{\partial \overline{w}}{\partial \overline{x}}\frac{\partial \overline{w}}{\partial \overline{y}} \right]\left[\frac{\partial \overline{w}}{\partial \overline{x}}\phi_i\psi'_j + \frac{\partial \overline{w}}{\partial \overline{y}}\phi_i'\psi_j \right] \right\} d\overline{x}\, d\overline{y}$$
$$= \frac{EhcL}{2(1-\nu^2)}\left(\frac{h}{c}\right)^4 F^{ij}$$

Acknowledgments

This work was supported by NASA Lewis Research Center, Grant NAG 3-724. G. L. Stefko was the Grant Technical Monitor. The authors would also like to acknowledge the careful and constructive review of the paper by M. A. Hopkins.

References

[1]Dowell, E. H., *Aeroelasticity of Plates and Shells*, Kluwer/Noordhoff International Publishing, Leyden, 1975.

[2]Dowell, E. H., "Nonlinear Oscillations of a Fluttering Plate," AIAA Journal, Vol. 4, No. 7, 1966, pp. 1267–1275.

[3]Dowell, E. H., "On Asymptotic Approximations to Beam Modal Functions," *Journal of Applied Mechanics*, Vol. 51, June 1984, p. 439.

[4]Dugundji, J., "Simple Expressions for Higher Vibration Modes of Uniform Euler Beams," AIAA Journal, Vol. 26, No. 8, 1988, pp. 1013–1014.

[5]Dowell, E. H., et al., *A Modern Course in Aeroelasticity*, 2nd ed., Kluwer Academic Publishers, Boston, 1989.

[6]Fralich, R. W., and Hedgepeth, J. M., "Flutter Analysis of Rectangular Wings of Very Low Aspect Ratio," NACA TN 4245, June 1958.

[7]Bisplinghoff, R. L., and Dugundji, J., "Influence of Aerodynamic Heating on Aeroelastic Phenomena," *High Temperature Effects in Aircraft Structures*, AGARDOGRAPH No. 28, edited by N. J. Hoff, Pergamon Press, New York, 1958, Chap. 14.